Robotics and Autonomous Systems 174 (2024) 104622

Contents lists available at ScienceDirect

Robotics and Autonomous Systems

journal homepage: www.elsevier.com/locate/robot

Modelling of Modular Soft Robots: From a Single to Multiple Building Blocks ☆

Mohamed G.B. Atia [a], Abdelkhalick Mohammad [a,*], Andres Gameros [a], Dragos Axinte [a], Iain Wright [b]

[a] Rolls-Royce UTC in Manufacturing and On-Wing Technology, The University of Nottingham, NG8 1BB, UK
[b] Rolls-Royce plc, Derby, DE24 8BJ, UK

ARTICLE INFO

Keywords:
Soft robotics
Dielectric elastomer actuators
Building blocks
Modelling
Reconfigurability
Modularity

ABSTRACT

Despite the advances in soft robots, their modelling is still one of the research challenges due to the complexity and non-linearity of their soft nature. A novel design of reconfigurable soft robots was recently introduced to bring more maturity to the field of soft robots. Here, a modelling study of the building blocks and the assembled soft robot is developed for a deeper understanding of the system and for predicting their behaviours. The model is validated using several sets of individual and multiple building blocks and the results show good tracking between the model and the experiments with reasonable errors. Towards adopting the model in robotic applications, a grasping setup of 2 assembled soft fingers is demonstrated where the model is used to predict the grasping force and compared to feedback sensing. The force prediction reveals the adaptability of the model and its robustness.

1. Introduction

Soft robotics is a growing field that can replace conventional robots [1] in applications where they are ineffective because of their several limitations such as the collision risk during human–robot interaction, the inflexibility of their structures for some operations and their reliance on conventional rigid materials and bulky electrical motors. Compared to conventional robots, the soft robots have the advantage of soft lightweight bodies, simple actuation mechanisms [2,3] (e.g. fluidic elastomeric actuators (FEAs) [4], shape memory alloy (SMA) [5], soft electromagnetic actuators [6], dielectric elastomer actuator (DEA) [7]) and ability to generate simple as well as complex movements. These different actuators provide soft robots with various flexible movements and alternatives for the same application.

DEA is a promising soft actuator [8] that has been widely used in soft robotic applications since it has simple design concepts, high efficiency [9], inexpensive components, and rapid response [10]. Additionally, DEAs have fast response (< 100 ms) and a resonant frequency of around 200 Hz [11]. The DEA consists of a thin (e.g. 5–200 μm) elastomer that is sandwiched between two stretchable electrodes [12]. Upon powering the electrodes with high voltage, the electrodes attract each other due to the opposite electrical charges, and they push the DEA towards the thickness and expand its surface area in the minimum energy directions [13]. In soft robots with DEA, usually, a pre-stretched DEA is attached to an elastic backbone and designed to perform a specific motion when the DEA is powered [14].

The modelling of soft robots with DEAs is an essential part of understanding their behaviours and for the sake of better design and control. The soft materials can develop large strains (e.g., up to 1000% [15]) which are nonlinear in relationship to the applied stresses therefore, predicting their behaviour is considered one of the main challenges in the modelling. For an accurate model, the non-linear mechanical properties of the soft robot need to be defined accurately. Several material models have been developed over the years to relate the stress and strain of the material, such as the Ogden model [16], the gent model [17], the Shariff model [18] and the Mooney model [19]. The Ogden model is one of the most accurate models and its accuracy is increased by increasing the number of parameters in the model. Another advantage is that it can describe the material behaviour along most of the working range of the material. While the gent model is much simpler but has less accuracy and working range [20].

Generally, the modelling is divided into analytical modelling [21] and numerical modelling [22]. Although numerical modelling is a convenient way to predict the behaviour of the soft robot, it is preferred to use the analytical model for simple structures as it consumes much less time compared to the numerical model. The analytical model can be used in real-time for quick prediction of the robot's behaviour and

☆ This research was funded by Rolls-Royce plc direct fund to the Rolls-Royce UTC, Nottingham (PO Number: 1500-00401149) and the University of Nottingham.
* Corresponding author.
E-mail addresses: Mohamed.Atia@nottingham.ac.uk (M.G.B. Atia), Abd.Mohammad1@nottingham.ac.uk (A. Mohammad), Andres.gameros@nottingham.ac.uk (A. Gameros), Dragos.axinte@nottingham.ac.uk (D. Axinte), Iain.wright@rolls-royce.com (I. Wright).

https://doi.org/10.1016/j.robot.2024.104622
Received 4 January 2023; Received in revised form 24 November 2023; Accepted 1 January 2024
Available online 11 January 2024

accurate predictive control [23]. The energy-based analytical modelling is considered one of the most effective approaches [24] to predict soft robot behaviours. The energy method is used to describe the relationship between energies of the system (i.e. DEA strain energy, DEA electrostatic energy, backbone strain energy, ...) [25,26] using the material models. It has been widely used for modelling different robotic designs, for example; static modelling to predict and design the soft robot behaviour, powered by DEA, [27] or for predicting the effect of the design parameters on the actuation strokes [28]. It can also be adopted for dynamic modelling such as the systems in [29, 30] which provided a maximum root-mean-square error between the model and experiments of around 10.78% and 3% respectively. Other models to predict the dynamic hysteresis of the DEA of a single cone structure [31] and double-cone [32] DEAs have achieved a maximum root-mean-squared error of 5.53% and a maximum prediction error of 10.6%, relatively.

In this paper, we present an analytical modelling method for the reconfigurable soft robots, actuated by DEA, and the building blocks that were recently developed by the authors in [33] for deeper understanding and predicting their behaviours. Using the energy method technique and the Ogden model of the material, the analytical model is developed not only to predict a robot's behaviour but also is demonstrated in specific robotic applications, e.g., a grasping robotic system to predict the grasping force, to prove the robustness of the system and its suitability for robotic applications.

This paper is organised as the following: a summary of the building blocks concept and research gaps are explained in Section 2. The analytical modelling of single and multiple building blocks is provided in Section 3. Section 4 presents the validation experiments of the model and a demonstration of the model using a robotic grasping system. Finally, the conclusion is summarised in Section 5.

2. Problem definition

2.1. Summary of the building blocks concept

The novel concept of the building blocks (i.e., robotic modules) was recently introduced by the authors in [33] that can be connected in series to assemble reconfigurable soft robots of different types and configurations such as robotic fingers, robotic elephant trunks and mobile robots.

Each block consists of; (i) a DEA as the main actuator (shown in 1 of Fig. 1(a)), (ii) electrical terminals that are connected to the sides of the DEA to power it with high voltage (H.V.) for actuation (shown in 2 and 8 of Fig. 1(a)), (iii) 3D-printed linking-caps that represent the robot structure (shown in 3 and 6 of Fig. 1(a)), (iv) snap-fit features built in the linking-caps (shown in 4 and 7 of Fig. 1(a)), and (v) two NiTi rods that represent the backbone (shown in 5 of Fig. 1(a)). Fig. 1(b) shows an assembled 3D configuration of 3 building blocks in non-actuated and actuated modes.

For an accurate model of the building block, its working principle needs to be explained first and it is summarised as follows: First, the building block structure is formed by attaching and gluing the two NiTi rods, of diameter D, into the corresponding holes of the linking-caps so that the active distance of the NiTi rods is L (i.e., the distance between the linking-caps from the inside). Then, a DEA is stretched planarly of stretching ratios λ_1 and λ_2 in the longitudinal and circumferential axes respectively as shown in Fig. 2(a). This pre-stretched DEA is wrapped carefully around the building block structure and glued to the linking-caps surfaces as shown in Fig. 2(b). After relaxation, the building block develops an initial bending angle θ_0 of the building block as a result of the input energy of the DEA stretching to NiTi rods structure as shown in Fig. 2(c) and (e). The electrodes are painted over each side of the DEA and connected to the electrical terminals separately to finalise the DEA concept as shown in Fig. 2(d) (note, the electrodes are not shown in the schematic for a clearer view). Once H.V. is applied to the

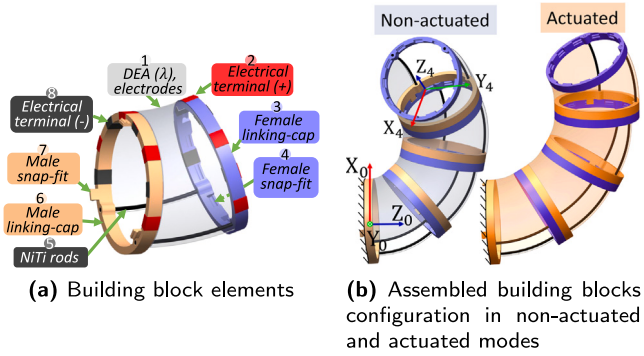

Fig. 1. The design of the building block.

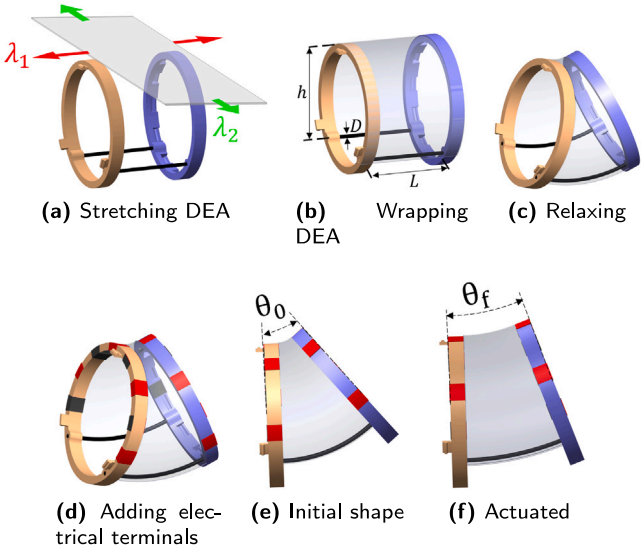

Fig. 2. A schematic of the manufacturing process.

electrical terminals (i.e., the two sides of the DEA), this input energy increases the strain of the DEA and therefore reduces the strain of the NiTi rods and the bending angle changes to rebalance the system energies as shown in Fig. 2(f). Thus, by changing the design parameters D, L, λ_1 and λ_2, different curvatures θ_0 of the building blocks can be obtained. This curvature will change upon the actuation when applying H.V. to the DEA.

2.2. Limitations and research gaps

Most of the state-of-art analytical models follow simple structure designs of the DEA such as planer DEAs [29] or conical DEA system [32]. Using analytical modelling, the developed models achieve between 3% to 10.6% maximum root-mean-squared error compared to the experiments. Usually, complex structures are modelled numerically using finite element methods for the sake of higher accuracy and to avoid the complexity of the analytical model.

The building blocks were previously modelled numerically using Abaqus by the authors [33] and the modelling has the following limitations; (I) it requires a relatively long time (approximately 30 min) to model one case of the building block (e.g., under specific stretching ratio and voltage). (II) The numerical modelling was not used to model the entire assembled robot, as it'll consume doubles the processing time of the individual building block, but was embedded in the kinematics robot model as individual modules. (III) The weights of the individual building blocks and the external loads affect the shape of the assembled

robot due to the system flexibility. These effects were not modelled in the previously developed numerical model, due to the expected long processing time. (IV) It is almost impossible to monitor or control a robotic system online, using the numerical model.

The primary contribution of this research work is developing an analytical modelling method for the complex structures of the soft robots assembled by the building blocks. This method is designed to tackle the mentioned limitations of the numerical modelling as follows:

1. The analytical model has a quick processing time while predicting the behaviour of the individual building blocks (to tackle limitation I) with maintaining good tracking of the robot behaviour comparable to the numerical modelling (The average error of the analytical model, of this work, is 7.34% while to the accuracy of the numerical modelling is 5.8% [33]).
2. For the assembled robot, the processing time of the analytical is also much less compared to the numerical modelling (to tackle limitation II). For example, an entire robot of 4 building blocks can consume approximately 0.4s to predict its behaviour using the analytical model.
3. The external loads and the weights of the building blocks are added to the analytical model to account for their effects (to tackle limitation III).
4. The analytical model can be used in different environments of the assembled robot (e.g., a grasping system) to predict, monitor or control its behaviour (to tackle limitation IV).

3. Analytical modelling

Here, the analytical modelling strategy of the single building blocks and the assembled robot is developed and explained. The energy method is used as the base of this model with the Ogden model to describe the dielectric elastomer (DE) material behaviour. The energy method has been widely used for analytically modelling soft robots. This method relies on defining the total energy of the robot, calculated as the summation of the energy of each element of the robot structure, and then solving the derivative of the total energy to the variable output (e.g., the bending angle).

3.1. Model of single building blocks

The DE is represented by a planar membrane of hyperelastic material with the dimensions (L_0, w_0, t_o) which is pre-stretched biaxially with stretching ratios λ_{pre1} and λ_{pre2} as shown in Fig. 3(a). Then, the DE is wrapped around the circular structure of the building block and it is assumed no energy losses occurred during this wrapping process as shown in Fig. 3(b). The multiplication of the stretching ratios in the 3 directions (λ_1, λ_2, λ_3) is equal to 1 due to the assumption of constant volume of the material as expressed in Eq. (1). Where λ_1 is the final stretching in the longitudinal direction, λ_2 is the final stretching in the circumferential direction, and λ_3 is the final stretching in the radial direction (i.e., thickness direction).

$$\lambda_1 \lambda_2 \lambda_3 = 1 \tag{1}$$

$$\lambda_3 = 1/(\lambda_1 \lambda_2) \tag{2}$$

There are two relaxations in the block; one along the λ_1 direction that is the result of the bending of the NiTi rods, and it can be expressed as in Eq. (3). The second relaxation is along the λ_2 which is the result of the relaxation of the membrane itself as it is not attached to anything from the sides. Assuming that the deflection along the λ_2 is negligible so it can be expressed in Eq. (4).

$$\lambda_1 = \lambda_{pre1} - f(\theta) \tag{3}$$

where f is a function of θ and calculated in the following.

$$\lambda_2 = \lambda_{pre2} \tag{4}$$

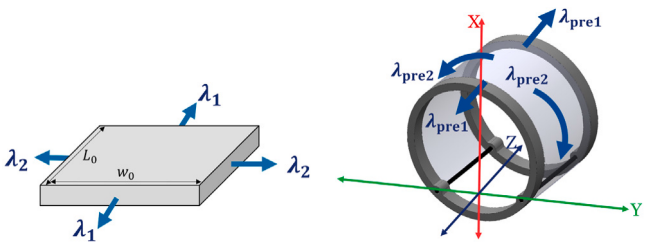

(a) Biaxial plane stretching **(b)** Wrapping the stretched DE

Fig. 3. The analytical model initialisation.

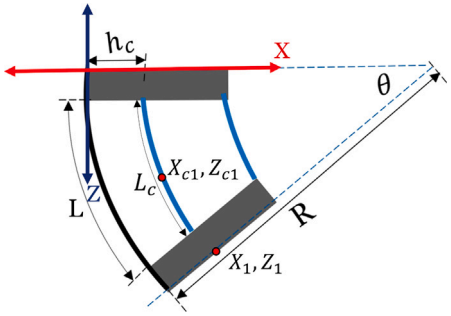

Fig. 4. The building block axes.

The deformation of the DEA along the linking-cap is inhomogeneous and to simplify the modelling, the average deformation is taking in consideration instead. In the previous research work [33] of modelling the building blocks numerically, the average DE thickness was adopted instead of modelling the thickness on every point of the DE and the results showed good tracing of the robot behaviour with an average error of approximately 5.8%. Hence, the average deformation of the DEA is considered acceptable in this modelling method. Assuming that the average final length of the DE, in the longitudinal direction, is L_c and it occurs at the centroid (h_c) of the DEA as shown in Fig. 4.

$$L_c = \lambda_1 L_0 \tag{5}$$

$$w = \lambda_2 w_0 \tag{6}$$

$$t = t_0/(\lambda_1 \lambda_2) \tag{7}$$

where w is the final width of the DE along the circumferential direction and t is the final thickness of the DE which occurs in the radial direction. These final values occur as a result of λ_1 and λ_2.

Since the length of the NiTi rod L is constant, it can be expressed as in Eq. (8). The deflection takes a circular curve of radius R as shown in Fig. 4 and expressed in Eq. (9):

$$L = L_0 \lambda_{pre1} \tag{8}$$

$$R = \frac{L}{\theta} \tag{9}$$

Since L_c is a shifted circular curve from the NiTi rods, it can be expressed in Eq. (10):

$$L_c = (R - h_c)\,\theta = \left(\frac{L}{\theta} - h_c\right)\theta = L - h_c\theta \tag{10}$$

L_c can be simplified by substituting Eqs. (3) and (8).

$$L_c = L_0 \lambda_{pre1} - h_c\theta = L_0\left(\lambda_{pre1} - \frac{h_c\theta}{L_0}\right) = L_0\lambda_1 \tag{11}$$

Then, the final longitudinal stretching (λ_1) can be expressed in Eq. (12) [34]. Therefore, $f(\theta) = \frac{h_c\theta}{L_0}$.

$$\lambda_1 = \lambda_{pre1} - \frac{h_c\theta}{L_0} \tag{12}$$

The Ogden model is used to describe the hyperelastic behaviour of the DE, and the energy density (W) is expressed in Eq. (13).

$$W = \sum_{i=1}^{n} \frac{\mu_i}{\alpha_i}(\lambda_1^{\alpha_i} + \lambda_2^{\alpha_i} + \lambda_3^{\alpha_i} - 3) \tag{13}$$

where μ_i and α_i are material parameters, while n represents the order of Ogden function as ($n = 1, 2, or 3$). The biaxial stresses in the directions of λ_1 and λ_2 are expressed in Eqs. (14) and (15) respectively.

$$\sigma_1 = \lambda_1 \frac{\partial W}{\partial \lambda_1} = \sum_{i=1}^{n} \mu_i(\lambda_1^{\alpha_i} - (\frac{1}{\lambda_1 \lambda_2})^{\alpha_i}) \tag{14}$$

$$\sigma_2 = \lambda_2 \frac{\partial W}{\partial \lambda_2} = \sum_{i=1}^{n} \mu_i(\lambda_2^{\alpha_i} - (\frac{1}{\lambda_1 \lambda_2})^{\alpha_i}) \tag{15}$$

The strain energy of the DEA can be expressed as ($U_{Strain} = Energy\ density * Volume$) as expressed in Eq. (16).

$$U_{Strain} = \sum_{i=1}^{n} \frac{\mu_i}{\alpha_i} \left(\lambda_1^{\alpha_i} + \lambda_2^{\alpha_i} + \lambda_3^{\alpha_i} - 3\right) L_0 L_{w0} t_0 \tag{16}$$

$$U_{Strain} = \sum_{i=1}^{n} \frac{\mu_i}{\alpha_i} \left(\lambda_1^{\alpha_i} + \lambda_2^{\alpha_i} + (\frac{1}{\lambda_1 \lambda_2})^{\alpha_i} - 3\right) L_0 L_{w0} t_0 \tag{17}$$

The electrostatic energy of the DEA can be expressed in Eq. (18).

$$U_{Ele} = \frac{\varepsilon_0 \varepsilon_r w L_c V^2}{2t} \tag{18}$$

where ε_0 is the permittivity of free space, ε_r is the dielectric constant of the DE material, V is the applied H.V. to the DEA, and t is the corresponding thickness of the DE at this state. Eq. (7) is used to substitute the value of t as in the following.

$$U_{Ele} = \frac{\varepsilon_0 \varepsilon_r w L_c V^2}{2t} = \frac{\varepsilon w L_c V^2 \lambda_1^2 \lambda_2^2}{2t_0} \tag{19}$$

Since the linking-caps are rigid, so the deflection of the structure occurs only in the NiTi rods and it is expressed as the strain energy of the NiTi rods U_{NiTi}. Although the equivalent reactional moment M can be calculated as expressed in Eq. (20).

$$M = \frac{E_{NiTi} I_{NiTi}}{L} \theta \tag{20}$$

where E_{NiTi} is the Young's modulus of the NiTi rods, and I_{NiTi} is the moment of inertia of the cross-sectional area of the two NiTi rods, of diameter D, and it is calculated from Eq. (21).

$$I_{NiTi} = 2\frac{\pi D^4}{64} = \frac{\pi D^4}{32} \tag{21}$$

The strain energy of the NiTi rods U_{NiTi} is expressed in Eq. (22).

$$U_{NiTi} = \frac{M^2 L}{2\ E_{NiTi}\ I_{NiTi}} = \frac{{E_{NiTi}}^2\ {I_{NiTi}}^2\ \theta^2\ L}{2\ L^2\ E_{NiTi}\ I_{NiTi}} = \frac{E_{NiTi}\ I_{NiTi}\ \theta^2}{2\ L} \tag{22}$$

Finally, the potential energy of the weight of the building block is ($U_{weight} = weight * Z_{c1}$). where Z_{c1} is Z distance of the centroid of the building block from the origin as shown in Fig. 4 (as this model for single building blocks) and can be derived from Eq. (33).

$$U_{weight} = weight * (Z_{c1}) = weight * (L_{Rigid} + \frac{L}{\theta} \sin(\frac{\theta}{2})) \tag{23}$$

where L_{Rigid} is length of the linking-cap, and θ is the bending angle of this building blocks. Similarly, if an external load (e.g., vertical force) is applied to the tip of the building block, its potential energy is $U_{load} = load * Z_1$.

$$U_{load} = load * (L_{Rigid} + \frac{L}{\theta} \sin(\theta)) \tag{24}$$

The total energy in the building block is expressed in Eq. (25) as the summation of the energies of Eqs. (17), (19), (22), (23) and (24).

$$U_{tot} = U_{Strain} - U_{Ele} + U_{NiTi} + U_{weight} + U_{load} \tag{25}$$

The model of single building blocks is the solution of minimising the first derivative of the total energy in Eq. (26).

$$\frac{dU_{Strain}}{d\theta} - \frac{dU_{Ele}}{d\theta} + \frac{dU_{NiTi}}{d\theta} + \frac{dU_{weight}}{d\theta} + \frac{dU_{load}}{d\theta} = 0 \tag{26}$$

In case of the building block is applying force upon actuation (e.g., blocked force or grasping forces), an additional term U_{Force} is added to the total energy as shown in Eq. (27). As the force F is applied to the tip point of the linking-cap and is perpendicular to the touch point, thus the energy can be calculated as in Eq. (28).

$$U_{tot} = U_{Strain} - U_{Ele} + U_{NiTi} + U_{weight} + U_{Force} \tag{27}$$

$$\begin{aligned} U_{Force} &= -(F_X X_1 + F_Z Z_1) \\ &= -(F\cos(\theta_0 + \theta_1 - \frac{\pi}{2})X_1 + F\sin(\theta_0 + \theta_1 - \frac{\pi}{2})Z_1) \end{aligned} \tag{28}$$

where X_1 and Z_1 are the X and Z distances of the endpoint of the building block (as this model for single building blocks). Note, that Eq. (28) calculates the energy of each component of the force. The two components of the force are F_X and F_Z and are calculated as $\{F\cos(\theta_0 + \theta_1 - \frac{\pi}{2}), F\sin(\theta_0 + \theta_1 - \frac{\pi}{2})\}$. Therefore, the model equation can be modified from Eq. (26) to be as in Eq. (29) to predict the robot building block behaviour.

$$\frac{dU_{Strain}}{d\theta} - \frac{dU_{Ele}}{d\theta} + \frac{dU_{NiTi}}{d\theta} + \frac{dU_{weight}}{d\theta} + \frac{dU_{Force}}{d\theta} = 0 \tag{29}$$

For a given design parameters of a building block (e.g., λ_1, D, L), a given external load, and a given input high voltage (V), the bending angle of the building block can be calculated by solving Eq. (29). It can be solved using MATLAB as a nonlinear function. Additionally, the model can be solved for any given variables to calculate an unknown parameter. This model was used to generate the look-up table of single building blocks that will be discussed in Section 4 and the validation comparison in Section 4.1.

3.2. Model of assembled soft robot

The robot model relies on the kinematics to define the location of the affecting loads and the centre of mass, therefore the robot kinematics [35] is introduced first. To further simplify the model, the kinematics are simplified for faster execution time.

The centreline of each building block consists of three connected lines; first a straight line representing the first linking-cap, then a circular curve representing the shifted bending of the NiTi rods, and finally a straight line representing the second linking-cap. Although, for the purpose of simplification, this structure can be further simplified and expressed by only a continuous curvature shape (i.e., the straight lines of the linking-caps are excluded and assumed curved). This assumption is valid because of the small length of the linking-caps compared to the entire length of the building block (i.e., a linking-cap is round 17% of the block length) and the respectively moderate range of bending angles of the NiTi rods (e.g., angles between 0°–30°). Thus, the curve length D_m at the centre of the building blocking m can be expressed in Eq. (30).

$$D_m = \theta_m * (\frac{L_m + 2L_{Rigid}}{\theta_m} - h) \tag{30}$$

where θ_m is the bending angle of the building block with the order m from the base, L_m is the NiTi rods length between the two linking-caps, h is the shifted distance between the curved NiTi rod and the centre of the building block (h = 8 mm in this design) and L_{Rigid} is the length of the linking-cap and is equal to 2.5 mm in this design as shown in Fig. 5.

Due to the assumption of constant curvature of the joining NiTi elements of the building block, the general transformation matrix of

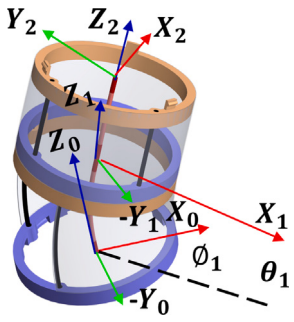

Fig. 5. The robot simple kinematics.

building block m can be derived as in Eq. (31):

$$P_m = \begin{bmatrix} X_m \\ Y_m \\ Z_m \end{bmatrix} = R_m \begin{bmatrix} \frac{D_m}{\theta_m}\cos(\phi_m)(1-\cos(\theta_m)) \\ \frac{D_m}{\theta_m}\sin(\phi_m)(1-\cos(\theta_m)) \\ \frac{D_m}{\theta_m}\sin(\theta_m) \end{bmatrix} + \begin{bmatrix} X_{m-1} \\ Y_{m-1} \\ Z_{m-1} \end{bmatrix} \tag{31}$$

$$R_m = R_{m-1} Rot_z(\phi_{m-1}) Rot_y(\theta_{m-1}) \tag{32}$$

As (X_m, Y_m, Z_m) is the coordinates of the endpoint of building block m and ϕ_m is the rotating angle of the building block around its local Y-axis and it is also called the direction angle.

Furthermore, the centroid of a building block m is located at the centre and on the centre line at an angle $(\frac{\theta_m}{2})$. The centroid location is needed as it's where the weight of the building block is represented. Therefore, the coordinates of the centroid (X_{cm}, Y_{cm}, Z_{cm}) of module m in the assembled robot can be extracted as expressed in Eq. (33).

$$P_{cm} = \begin{bmatrix} X_{cm} \\ Y_{cm} \\ Z_{cm} \end{bmatrix} = R_m \begin{bmatrix} \frac{D_m}{\theta_m}\cos(\phi_m)(1-\cos(\frac{\theta_m}{2})) \\ \frac{D_m}{\theta_m}\sin(\phi_m)(1-\cos(\frac{\theta_m}{2})) \\ \frac{D_m}{\theta_m}\sin(\frac{\theta_m}{2}) \end{bmatrix} + \begin{bmatrix} X_{m-1} \\ Y_{m-1} \\ Z_{m-1} \end{bmatrix} \tag{33}$$

Now, regarding the modelling of the assembled robot. Assuming that the building blocks {1, 2, . . . , m} are connected in series, the model of this assembly can derived from Eq. (25) as the summation of the energies of all the blocks as expressed in Eq. (34).

$$U_{tot} = U_{Strain,1} - U_{Ele,1} + U_{NiTi,1} + U_{weight,1} + U_{Strain,2} - U_{Ele,2} + \cdots + U_{NiTi,m} + U_{weight,m} + U_{load} \tag{34}$$

The model of the assembled robot of multiple building blocks is the solution of minimising the first derivative of the total energy as shown in Eq. (35).

$$\frac{dU_{tot}}{d\theta_1} = 0, \quad \frac{dU_{tot}}{d\theta_2} = 0, \quad \ldots, \quad \frac{dU_{tot}}{d\theta_m} = 0 \tag{35}$$

where the DEA strain energies of each block are calculated similar to Eq. (17), the electrostatic energy of each block is calculated similar to Eq. (18), the NiTi rod strain energy in each block is calculated similar to Eq. (22) and the potential energy of the weights of the building blocks occur in the middle of each module (i.e., for module m its weight occurs at $\frac{\theta_m}{2}$) and can be expressed as:

$$\begin{aligned} U_{weight,1} &= weight * Z_{c1} \\ U_{weight,2} &= weight * Z_{c2} \\ &\vdots \\ U_{weight,m} &= weight * Z_{cm} \end{aligned} \tag{36}$$

Similarly, the potential energy of an external load on the tip (i.e., the last linking-cap of the module m) can be expressed as:

$$U_{load} = load * Z_m \tag{37}$$

And in the case of forces generated from the building block, Eq. (34) can be modified by replacing the U_{load} by U_{Force} similar to the previously discussed model in Eq. (27). Thus, U_{Force} can be defined as in Eq. (38), as $\{F_X, F_Y, F_Z\}$ are the force components generated on the robot tip.

$$U_{Force} = -(F_X X_m + F_Z Z_m + F_Y Y_m) \tag{38}$$

The model in Eq. (35) can be used to predict the behaviour of the robot assembled by specific building blocks which their design parameters are known. This model consists of m number of equations so it can calculate a maximum number of unknowns up to m using the nonlinear solvers of MATLAB. For example, if all the robot variables, including the voltage, are known, the model can be solved to calculate the bending angles $\{\theta_1, \theta_2, \ldots, \theta_m,\}$ of building blocks assembled in the robot. This case can be shown in validation comparison in Section 4.2.

Similarly in the case of the robot is not moving and generating forces on a surface. The resulted forces from the robot can be calculated from the same equations for a given input voltage and a fixed bending angle. This case will be presented in Section 4.3.

4. Experiments and validation

Here, the validation experiments of the analytical model is discussed in detail in two sets of experiments; using single building blocks, and multiple building blocks. The model parameters are tuned to better track the system performance. The modelling method can be applied in soft robot application such as for predicting grasping force of assembled soft fingers. Before going through the validation process, it's needed to mention the look-up table obtained from the model.

To guide the assemble of building blocks into different configurations, a look-up table is developed with 84 possible designs to select the suitable building blocks curvature based on the corresponding design parameters (D, L and λ_1). These specific parameters values are selected to generate a wide range of bending angles (approximately from 3° to 30°) for the building blocks. Note that a constant relationship is established between λ_1 and λ_2 that $\lambda_1\lambda_2 = 2.5$ to reduce the independent parameters.

As proven by finite element modelling in [33], they are the key three parameters that affect the curvature, stroke and stiffness of the building block directly. Their effects can be summarised as follows; (i) Increasing λ_1 increases the initial bending angle, (ii) Increasing the D reduces the initial bending angle and reduces the stroke and the stiffness of the block, (iii) Increasing L increases the initial bending angle and increases the stroke but reduces the stiffness of the building block.

The design parameters used for generating the look-up table are listed as follows:

- L is the distance between the two linking-caps and it has the following values {10, 12.5, 15} mm.
- λ_1 is the stretching ratio of the DEA in the axial direction and it has seven values as follows {1.5, 1.6, 1.7, . . . , 2.1}.
- D is the NiTi rod diameter and it has four values as follows {0.31, 0.44, 0.62, 0.763} mm.

Other design parameters, such as the outer diameter of the linking-caps, could be considered but kept constant in this research because they could change the design fundamentally. If the outer diameter is considered as a key design parameter, it'll be hard to connect or assemble different building blocks together.

4.1. Validation of single building blocks

In these experiments, the analytical model is validated using 9 individual building blocks in terms of the bending angle behaviour for an applied range of high voltages and external loads. The variable inputs to the experiments are:

Table 1
The D-optimal IDs.

ID	D (mm)	L (mm)	λ_1
4	0.31	10	1.8
8	0.31	12.5	1.5
15	0.31	15	1.5
22	0.44	10	1.5
35	0.44	12.5	2.1
39	0.44	15	1.8
43	0.62	10	1.5
53	0.62	12.5	1.8
63	0.62	15	2.1

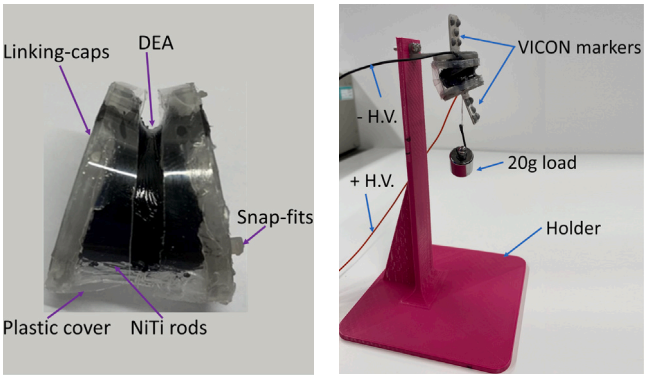

(a) Manufactured building block **(b)** The setup under 20g calibrated weight.

Fig. 6. The validation setup of single blocks.

- Voltage: which ranges from 0 to 2.8 kV.
- Load: external calibrated weights of {0 g, 2 g, 5 g, 10 g, 20 g} are used to apply vertical force load. Note that there is an additional external load of 1 g which is the weight of the VICON markers on the tip of the building blocks. Therefore the external loads applied become {1 g, 3 g, 6 g, 11 g, 21 g}.
- Building block IDs: it is challenging to perform the validation experiments for all the 84 cases in the look-up table, even if the levels of the three key design parameters (stretching ratio, NiTi diameter, NiTi length) are reduces to three values only, it requires 3^3 cases of experiments. Therefore a design experiment is performed to optimise the IDs to the most effective IDs that if used in the experiments will present a full description of the parameters effects.
  Only three levels of the three key design parameters, as below, are investigated in the optimisation and are implemented in the Minitab software [36] using the D-optimal approach to reduce the number of experiments:
  - Stretching ratio λ_1 : has three values {1.5, 1.8, 2.1}.
  - NiTi diameter D: has three values {0.31, 0.44, 0.62} mm.
  - NiTi length L: has three values {10, 12.5, 15} mm.

  The results of D-optimal approach are 9 IDs with the most effect on the performance without duplicating the effects and they are shown in Table 1.

The experimental setup is shown in Fig. 6 where VICON measurement system (also in Fig. 11) is used with the markers placed on the two linking-caps of the building block. The base (one linking-cap) of building block is fixed vertically while the tip (the other linking-cap) is attached to the load.

Due to the manufacturing errors, the model has an average error of 16%. Therefore, additional 3 parameters are identified to tune the model.

Table 2
The tuned model parameters.

Parameter	Value	Definition
E_{NiTi}	50.2353 GPa	NiTi Young's modulus
$A_{\lambda,1}$	0.9552307	Stretching ratio λ_1 accuracy
$A_{\lambda,2}$	0.910246	Stretching ratio λ_2 accuracy

Table 3
The other model parameters "Not changed".

Symbol	Value	Description
μ_1	0.0968 MPa	Ogden model parameter
μ_2	0.149 MPa	Ogden model parameter
μ_3	0.0115 MPa	Ogden model parameter
α_1	2.8639	Ogden model parameter
α_2	3.23882	Ogden model parameter
α_3	4.450305	Ogden model parameter
ϵ_r	2.0	DEA permittivity (ELASTOSIL 2030)
R	25 mm	The outer diameter of the Linking-caps
h	20.5 mm	Height of the NiTi rods to the top of the linking-cap
L_{Rigid}	2.5 mm	Width of the linking-cap

- NiTi Young's modulus: as the measured values range from 39 GPa to 53 GPa (using previously performed stress/strain tests), but it will be tuned here to find an optimised value instead.
- Stretching ratio λ_1 accuracy due to the manual stretching errors. The value of the stretching is updated by multiplication with constant parameter ($A_{\lambda,1}$).
- Stretching ratio λ_2 accuracy due to the manual stretching errors. The value of the stretching is updated by multiplication with constant parameter ($A_{\lambda,2}$).

The tuned model parameters are summarised in Table 2. The tuning process [37] is done by optimising these parameters (using Particle Swarm Optimisation [38,39]) to minimise the accumulative error of all the points (565 points) of the experiments shown in Fig. 7. The other untuned parameters are listed in Table 3.

A sample of the comparison between the experiments and the model with optimised parameters is shown in Fig. 7. The results of the building block of ID 4 (the smallest NiTi rod diameter) show good tracing of the whole behaviour along the input voltage but there is a total shift of the behaviour with a specific angle that increases with increasing the load. In other words, the error is minimum under no external load, while it increases with increasing the load. This behaviour can be the result of the simplified assumptions of the model such as NiTi rods are elastic and, the ignored effect of the shear forces on the NiTi rods as it is assumed that only bending occurs. Similarly, the behaviour of IDs 8 (shown in Fig. 7(a)) and 15 as they have the same NiTi rod diameter.

For the case of IDs 22 (shown in Fig. 7(b)), 35 and 39 (shown in Fig. 7(c)), they have the same diameter and similar behaviour in terms of the shifting angle between the experiments' behaviours and the model behaviour for the different external loads. Similarly, the IDs of 43, 53 and 63 (shown in Fig. 7(d)) have a similar shifting angle which is almost constant with the different loads. Thus, this shifting angle is variable for the small NiTi rod diameters and almost constant for the higher NiTi rod diameters.

The absolute average error of all the points (565 points) of the model is 7.34% with maximum absolute error of 25% and minimum error of 0.032%. The main reason of this value of errors is that the wide range of design cases (i.e., different NiTi diameters and lengths and different stretching ratios) that is used in the model. Although, this error can be significantly reduced by tuning the parameters in Table 2 using fewer designs for a smaller range of designs.

Note that for the tuning of the model, only the first set of experiments of single building blocks (single building blocks), not the second set (multiple building blocks), was used because the measurements

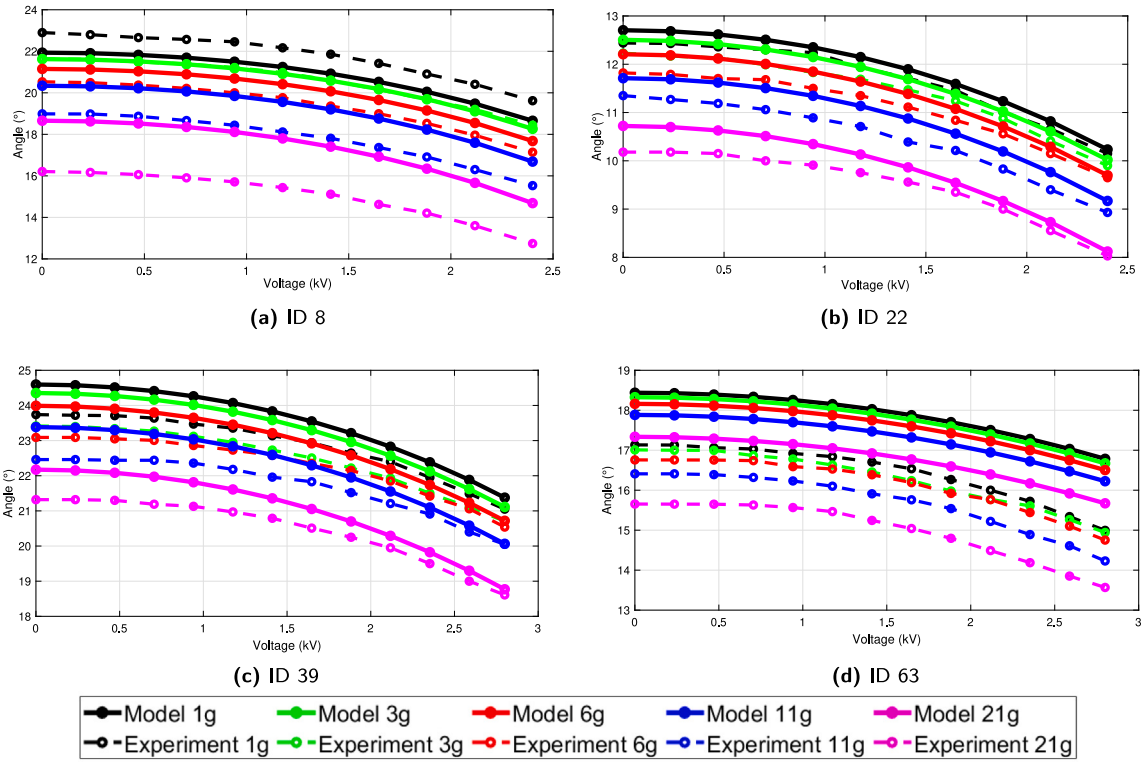

Fig. 7. The analytical model validation of single building blocks.

Table 4
A sample of the look-up table structure.

ID	D (mm)	L (mm)	λ_1	θ_0 (°)
1	0.31	10	1.5	14.84°
2	0.31	10	1.6	15.83°
3	0.31	10	1.7	16.74°
...	...	...	...	...
7	0.31	10	2.1	19.64°
8	0.31	12.5	1.5	18.55°
...	...	...	...	...
21	0.31	15	2.1	29.46°
22	0.44	10	1.5	12.58°
...	...	...	...	...
46	0.62	10	1.8	9.24°
47	0.62	10	1.9	10.28°
...	...	...	...	...
83	0.763	15	2.0	10.18°
84	0.763	15	2.1	11.37°

of the second set of experiments may be affected by the clearance between the assembled building blocks which will lead to an inaccurate description of the behaviour.

A sample of the look-up table structure is shown in Table 4 generated from the analytical model with the optimised parameters.

4.2. Validation of multiple building blocks (soft robot)

To validate the robot structure consisting of multiple building blocks assembled together, three configurations ($Conf_{63,35,4}$, $Conf_{43,39,15}$ and $Conf_{63,43,39,22,15,4}$) of the previous single blocks are experimented and evaluated in terms of the bending angle for the same defined external calibrated loads. The experiments of these configurations are compared to the analytical model with the optimised parameters.

Configuration $Conf_{63,35,4}$ consists of 3 building blocks connected in a series of IDs {63, 35, 4} from the base to tip, similarly configuration $Conf_{43,39,15}$ consists of 3 building blocks but of different IDs {43, 39, 15} from the base to tip. These specific IDs are selected from Table 1 to have different NiTi rod diameters, lengths and stretching ratios at the same configuration to cover a wide range of the model validation. Configuration $Conf_{63,43,39,22,15,4}$ consists of 6 blocks connected in a series of IDs {63, 43, 39, 22, 15, 4} from the base to the tip as shown in Fig. 11. These specific IDs contain the largest and smallest lengths for each NiTi rod diameter to have a variety of design parameters in this configuration.

The inputs to the experiments and the model are the same as the previous experiments of the single blocks validation. These inputs are; voltage from 0 to 2.8 kV, an external load of {1 g, 3 g, 6 g, 11 g, 21 g} and the selected building blocks IDs based on the D-optimal approach (discussed in the previous section). The output of these comparisons is the (accumulative) bending angle of the entire assembled robot.

The comparisons between the experiments and the model of configurations $Conf_{63,35,4}$, configuration $Conf_{43,39,15}$, and $Conf_{63,43,39,22,15,4}$ are shown in Figs. 8(a), 9(a) and 10(a), respectively. In configuration $Conf_{63,35,4}$, the model behaviour matches the experiment behaviour of the robot but is shifted with an error angle as shown in Fig. 8(b). This shift resembles the accumulative error of each building block and it increases by increasing the external load (e.g., there is an increase of 1° between the error of adding more external loads). Similarly, configuration $Conf_{43,39,15}$ shows good tracing behaviour but the error increases with increasing the input voltage (e.g., it has about −2° error at no voltage input but has around −5.5° error at 2.8 kV under 3 g load as shown in Fig. 9(b)) due to the accumulative error of each building block, unlike configuration $Conf_{63,35,4}$. Configuration $Conf_{63,43,39,22,15,4}$ has a good tracing along the voltage but the error increases with the increased voltage (e.g., the error increases approximately 6.6° when applying 2.8 kV). The average error of configurations $Conf_{63,35,4}$, $Conf_{43,39,15}$, and $Conf_{63,43,39,22,15,4}$ is 10.6%, 5.36% and 3.55% respectively. It is worth mentioning that the assembly error of the snap-fit is not included in the model which has mechanical clearances that can affect the total error of the assembly.

The increasing error of the three configurations with increasing voltage is expected due to the increased resistance of the robot which increases the energy consumption which was not included in the model

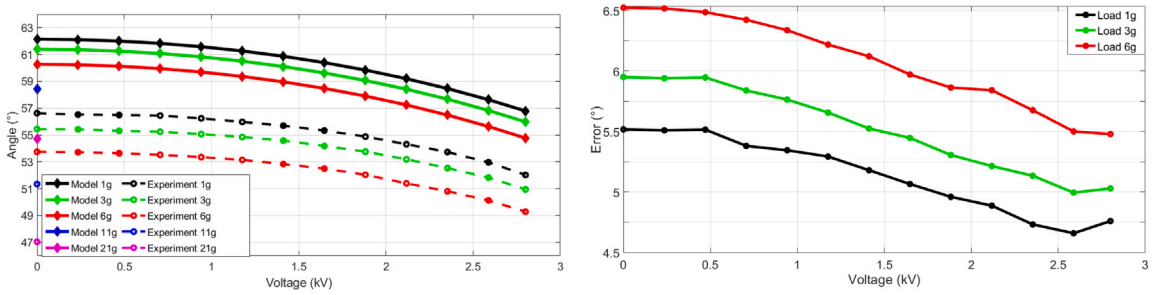

(a) Angle Vs. Voltage **(b)** Angle error

Fig. 8. The analytical model validation of configuration $Conf_{63,35,4}$.

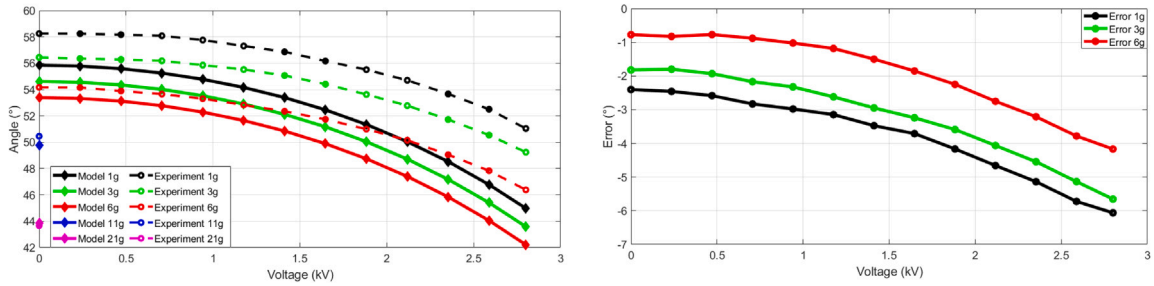

(a) Angle Vs. Voltage **(b)** Angle error

Fig. 9. The analytical model validation of configuration $Conf_{43,39,15}$.

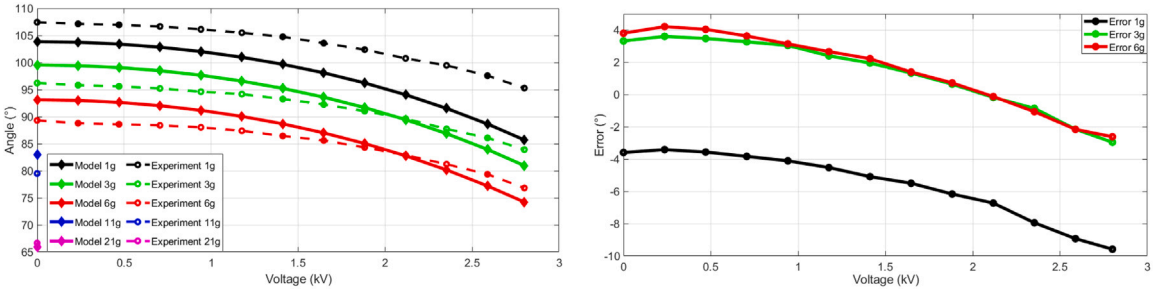

(a) Angle Vs. Voltage **(b)** Angle error

Fig. 10. The analytical model validation of configuration $Conf_{63,43,39,22,15,4}$.

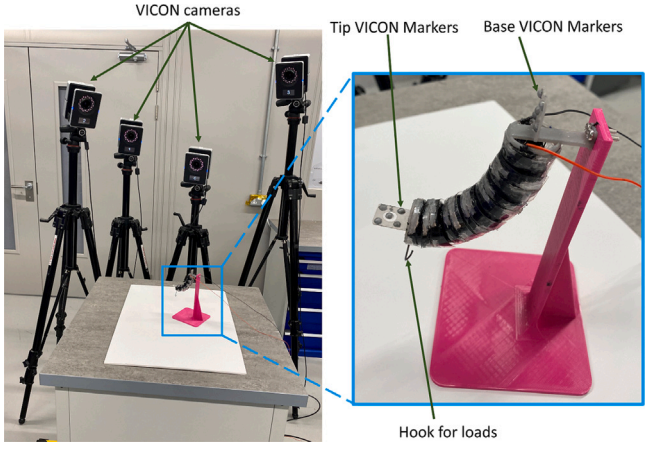

Fig. 11. The experimental set up of the analytical model validation of assembled modules.

for simplifying the system model. For example in the experiment, adding more building blocks to the robot reduces the working voltage of the added block as the power is affected by the total resistance of the previous blocks. Therefore the power (effective voltage) transferred to the added blocks is reduced and thus the behaviour is different, but it is assumed to be neglected as the building block number in the robot used in the verification is 3–6 blocks. Furthermore, the electrode thickness have a negative effect on the robot's behaviour which was not included in the model because of the difficulties of measuring their thicknesses in the 3D structure of the building block.

Overall, the analytical model provides a good tracing of the single building block structures and the different assembled configurations of multiple building blocks connected in a series (e.g., 3 building blocks and 6 building blocks configurations).

4.3. Case study: Prediction of grasping force

An application of the reconfigurable robot is soft fingers for grasping [33]. A crucial advantage of this concept is the capability of being assembled into different configurations with different payload capacities. Hence, a robot configuration can be built for desired payload

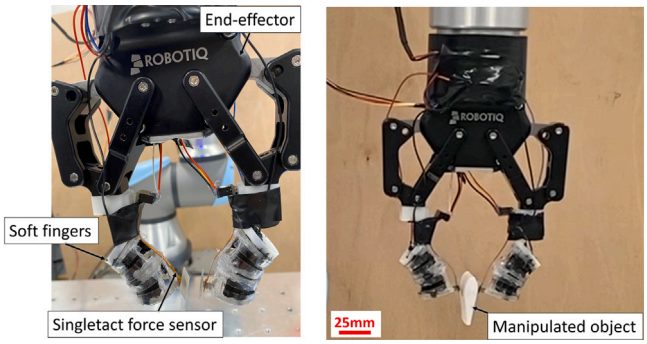

(a) The grasping setup and components.

(b) Snapshot during grasping the object

Fig. 12. The grasping system (using 2 soft fingers) for predicting the grasping forces.

to the application for an energy efficient solution. An 8 g object has been selected in this case study to simulate the case of grasping delicate objects.

The analytical model is used for predicting the assembled robot forces for further control or system monitoring (i.e., manipulation forces). In this experiment, 2 soft fingers are assembled and each finger consists of 2 building blocks of IDs 36. Delicate force sensors (singletact sensor 1N force) are attached to the tip of each soft finger, to measure the actual grasping forces to evaluate the model measurements as shown in Fig. 12.

The model is solved using MATLAB as a nonlinear system. The grasping force is calculated following the flowchart in Fig. 13 (similar to [40]). First, using the design parameters of the soft finger are used to identify its initial bending angles using the analytical model at Zero voltage. Then, the voltage is incremented while checking from the model that the output P_{tip2} doesn't collide with the object's surface. To calculate P_{tip2}, the bending angle is calculated from Eqs. (39) and (40) then, the P_2 is calculated according to the robot kinematics from Eq. (31) then, the body tip point P_{tip2} can be calculated easily based on the linking-cap rigid structure.

$$U_{tot} = U_{Strain,1} - U_{Ele,1} + U_{NiTi,1} + U_{weight,1} + U_{Strain,2} - U_{Ele,2} + U_{NiTi,2} + U_{weight,2} \tag{39}$$

$$\frac{dU_{tot}}{d\theta_1} = 0, \quad \frac{dU_{tot}}{d\theta_2} = 0 \tag{40}$$

When the soft finger tip touches the object surface, the angles θ_1, θ_2 are kept fixed with their last values and the grasping force F_{gr} is calculated from Eq. (42) as its the only unknown in this equation. Note that the strain energy of the grasping U_{grasp} is added to the total strain energy as expressed in Eq. (41) similar to Eq. (29).

$$U_{tot} = U_{Strain,1} - U_{Ele,1} + U_{NiTi,1} + U_{weight,1} + U_{Strain,2} - U_{Ele,2} + U_{NiTi,2} + U_{weight,2} + U_{grasp} \tag{41}$$

$$\frac{dU_{tot}}{d\theta_1} = 0, \quad \frac{dU_{tot}}{d\theta_2} = 0 \tag{42}$$

$$U_{grasp} = -(F_{gr}X_2\cos(\theta_0 + \theta_1 + \theta_2 - \frac{\pi}{2}) + F_{gr}Z_2\sin(\theta_0 + \theta_1 + \theta_2 - \frac{\pi}{2})) \tag{43}$$

where θ_0 is the rotation angle of the robot base, θ_1 and θ_2 are the initial bending angles of the first and second modules respectively from the top and F_{gr} is the grasping force.

The grasping force is satisfied once the F_{gr} is equal to or greater than F_{req} which refers to the required force to grasp an object and it can be calculated from the contributed weight of the object (i.e., if two

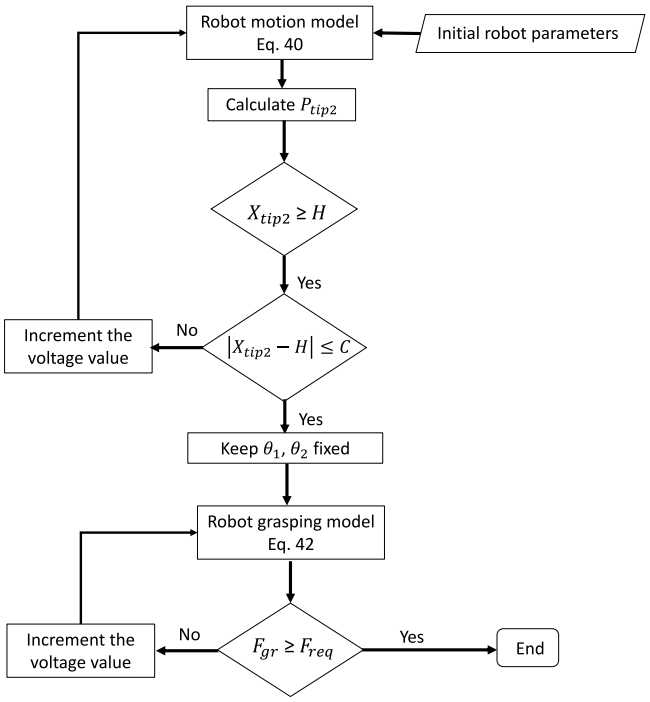

(a) Flowchart of the grasping method

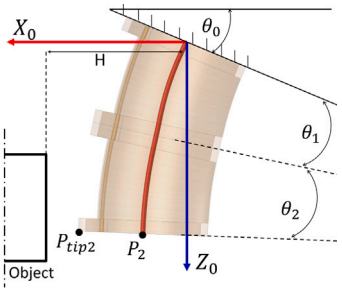

(b) Grasping setup

Fig. 13. Calculation of the grasping force.

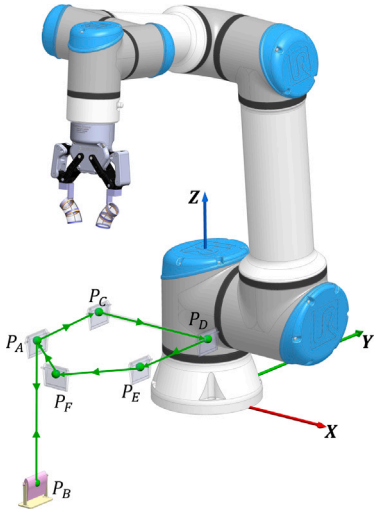

Fig. 14. The soft gripper path using the robot manipulator during the experiment.

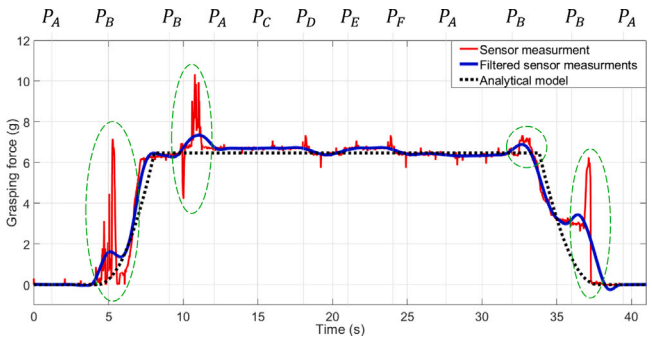

Fig. 15. Comparison between the model vs. measurements of the sensor.

fingers are used for grasping, then each finger holds half of the weight) and the friction coefficient $\mu_{friction}$ is as expressed in Eq. (44).

$$F_{req} = \frac{ObjectWeight}{N_f \ \mu_{fr}} = 0 \tag{44}$$

where N_f is the number of fingers contributed to grasping the object and μ_{fr} is the friction coefficient between the finger and the object at the grasping region.

This demonstration experiment of the grasping force is performed using the robot manipulator and the two-fingers robot to investigate the robustness of the grasping system for a time period of approximately 30 s (as shown in Movie S0, Supporting Information). The path of the soft fingers (i.e., soft gripper) during the experiment is shown in Fig. 14. Fig. 15 shows the grasping force of the assembled soft fingers and the filtered measurements using the Lowess Smoothing filter during the grasping. It shows the experiment and the model behaviour of the grasping force F_{gr} with a good match. It has been noted that there is a peak force just before the grasping when the fingers are surrounding the object and another peak during placing the object due to the disturbance from the object holder. Also, it reveals that the peak of the grasping force in the experiment occurs when the robot manipulator changes its position along the Z-axis (gravitational axis), which happens due to the object inertia component in this direction. This can be seen at the seconds of 5, 12, 32 and 37 as the acceleration/deceleration affects the weight of the object and therefore the grasping forces. Since the model is static, it can't predict these changes, but this will be part of the future work.

Fig. 16 shows snapshots during the demonstration as follows. First, the robot manipulator is on top of the object (its home position at position P_A) while the soft fingers are deactivated as shown in Fig. 16(a). Then, the robot manipulator approaches the object at position P_B as shown in Fig. 16(b), after that, the soft fingers are actuated according to the flowchart in Fig. 13 while the robot manipulator not moving (stand still at position P_B) as shown in Fig. 16(c). Once the soft robot has reached its desired force, the robot manipulator moves upwards to position P_A as shown in Fig. 16(d). Additionally, the robot manipulator moves discrete displacements into different positions P_C, P_D and P_E, as in Fig. 16(e), (f) and (g), and moves with rotation angles to another position P_F such as in Fig. 16(h) and it returns to the initial position P_A as shown in Fig. 16(i). These additional movements (P_C, P_D, P_E and P_F) show how robust it is. Then, the robot manipulator moves to the object holder position P_B to place it as shown in Fig. 16(j) and waits till the soft fingers are deactivated to release the object (Fig. 16(k)). Finally, the robot manipulator returns to its home position P_A as shown in Fig. 16(l).

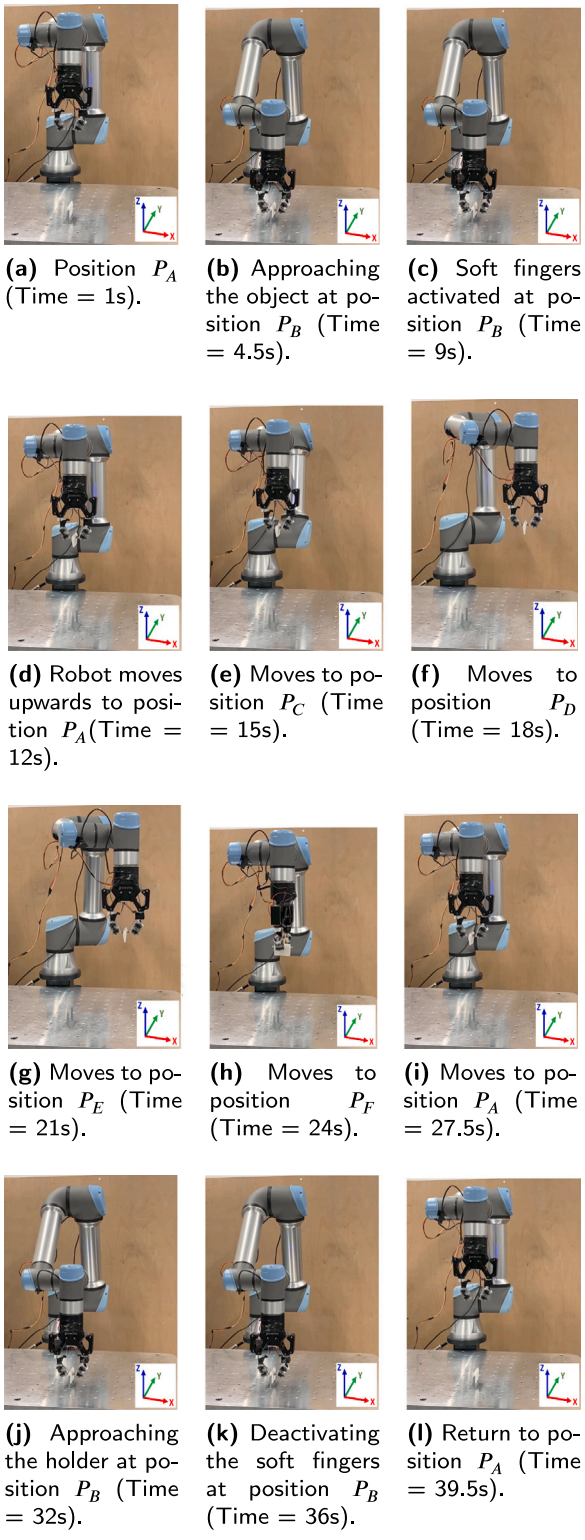

(a) Position P_A (Time = 1s). **(b)** Approaching the object at position P_B (Time = 4.5s). **(c)** Soft fingers activated at position P_B (Time = 9s).

(d) Robot moves upwards to position P_A(Time = 12s). **(e)** Moves to position P_C (Time = 15s). **(f)** Moves to position P_D (Time = 18s).

(g) Moves to position P_E (Time = 21s). **(h)** Moves to position P_F (Time = 24s). **(i)** Moves to position P_A (Time = 27.5s).

(j) Approaching the holder at position P_B (Time = 32s). **(k)** Deactivating the soft fingers at position P_B (Time = 36s). **(l)** Return to position P_A (Time = 39.5s).

Fig. 16. Snapshots of the robot manipulator positions during grasping demonstration.

5. Discussion and conclusion

This research work introduces an analytical modelling strategy of building blocks and assembled reconfigurable soft robots which was recently presented by the authors. The developed model is validated using two sets of experiments where the building blocks are under different high voltage values and different gravitational loads. The first set consists of 9 individual building blocks and they were used for tuning the model parameters to minimise the average error up to

7.34%. The second set consists of three configurations assembled of 3 building blocks, other 3 building blocks and 6 building blocks where the average error was 10.6%, 5.36% and 3.55%, respectively.

Furthermore, the analytical model is implemented in a grasping system to validate its accuracy and adaptability for robotic applications. Two grasping soft fingers, with delicate commercial sensors for feedback, are targeted to pick up and place an 8 g object. The comparison between the model and the feedback sensing is reasonable predictability and shows its opportunities for future applications (e.g., continuum soft robots and mobile robots). The future work will include dynamic modelling of the building blocks and the soft robot to deeply investigate and accurately control its dynamic behaviour. This dynamic modelling also includes the modelling of the different DEA viscoelastic materials (i.e., Acrylic based such as VHB 4910).

CRediT authorship contribution statement

Mohamed G.B. Atia: Conceptualization, Formal analysis, Investigation, Methodology, Validation, Visualization, Writing – original draft, Writing – review & editing. **Abdelkhalick Mohammad:** Conceptualization, Investigation, Supervision, Writing – review & editing. **Andres Gameros:** Conceptualization, Investigation, Supervision, Writing – review & editing. **Dragos Axinte:** Conceptualization, Investigation, Supervision, Writing – review & editing. **Iain Wright:** Funding acquisition.

Declaration of competing interest

The authors declare the following financial interests/personal relationships which may be considered as potential competing interests: Abdelkhalick Mohammad reports financial support was provided by Rolls-Royce plc.

Data availability

No data was used for the research described in the article.

Appendix A. Supplementary data

Supplementary material related to this article can be found online at https://doi.org/10.1016/j.robot.2024.104622.

References

[1] A.-D. Pham, H.-J. Ahn, High precision reducers for industrial robots driving 4th industrial revolution: state of arts, analysis, design, performance evaluation and perspective, Int. J. Precis. Eng. Manuf.-Green Technol. 5 (4) (2018) 519–533.

[2] J. Shintake, V. Cacucciolo, D. Floreano, H. Shea, Soft robotic grippers, Adv. Mater. 30 (29) (2018) 1707035.

[3] S. Zaidi, M. Maselli, C. Laschi, M. Cianchetti, Actuation technologies for soft robot grippers and manipulators: A review, Curr. Robot. Rep. (2021) 1–15.

[4] T. Wang, Y. Zhang, Y. Zhu, S. Zhu, A computationally efficient dynamical model of fluidic soft actuators and its experimental verification, Mechatronics 58 (2019) 1–8.

[5] J. Sheng, D. Gandhi, R. Gullapalli, J.M. Simard, J.P. Desai, Development of a meso-scale SMA-based torsion actuator for image-guided procedures, IEEE Trans. Robot. 33 (1) (2016) 240–248.

[6] T.N. Do, H. Phan, T.-Q. Nguyen, Y. Visell, Miniature soft electromagnetic actuators for robotic applications, Adv. Funct. Mater. 28 (18) (2018).

[7] S. Shian, K. Bertoldi, D.R. Clarke, Dielectric elastomer based "grippers" for soft robotics, Adv. Mater. 27 (43) (2015) 6814–+.

[8] E. Hajiesmaili, D.R. Clarke, Dielectric elastomer actuators, J. Appl. Phys. 129 (15) (2021) 151102.

[9] S.M. Ha, W. Yuan, Q. Pei, R. Pelrine, S. Stanford, Interpenetrating polymer networks for high-performance electroelastomer artificial muscles, Adv. Mater. 18 (7) (2006) 887–891.

[10] B. Rechenbach, M. Willatzen, B. Lassen, Theoretical study of the electromechanical efficiency of a loaded tubular dielectric elastomer actuator, Appl. Math. Model. 40 (2) (2016) 1232–1246.

[11] J.-H. Youn, S.M. Jeong, G. Hwang, H. Kim, K. Hyeon, J. Park, K.-U. Kyung, Dielectric elastomer actuator for soft robotics applications and challenges, Appl. Sci. 10 (2) (2020) 640.

[12] N. Sriratanasak, D. Axinte, X. Dong, A. Mohammad, M. Russo, L. Raimondi, Tasering twin soft robot: A multimodal soft robot capable of passive flight and wall climbing, Adv. Intell. Syst. 4 (12) (2022) 2200223.

[13] A. Khurana, A. Kumar, A.K. Sharma, M. Joglekar, Dynamic modeling of dielectric elastomer-based minimum energy structures with membrane entanglements and finite extensibility, Sādhanā 47 (3) (2022) 1–10.

[14] Y. Guo, L. Liu, Y. Liu, J. Leng, Review of dielectric elastomer actuators and their applications in soft robots, Adv. Intell. Syst. 3 (10) (2021) 2000282.

[15] C. Keplinger, T. Li, R. Baumgartner, Z. Suo, S. Bauer, Harnessing snap-through instability in soft dielectrics to achieve giant voltage-triggered deformation, Soft Matter 8 (2) (2012) 285–288.

[16] R.W. Ogden, Large deformation isotropic elasticity–on the correlation of theory and experiment for incompressible rubberlike solids, Proc. R. Soc. Lond. Ser. A Math. Phys. Eng. Sci. 326 (1567) (1972) 565–584.

[17] A.N. Gent, A new constitutive relation for rubber, Rubber Chem. Technol. 69 (1) (1996) 59–61.

[18] M. Shariff, Strain energy function for filled and unfilled rubberlike material, Rubber Chem. Technol. 73 (1) (2000) 1–18.

[19] M. Mooney, A theory of large elastic deformation, J. Appl. Phys. 11 (9) (1940) 582–592.

[20] M. Wissler, E. Mazza, Mechanical behavior of an acrylic elastomer used in dielectric elastomer actuators, Sensors Actuators A 134 (2) (2007) 494–504.

[21] A. Poulin, S. Rosset, H. Shea, Fully printed 3 microns thick dielectric elastomer actuator, in: Electroactive Polymer Actuators and Devices (EAPAD) 2016, Vol. 9798, SPIE, 2016, pp. 36–46.

[22] X. Cao, M. Zhang, Z. Zhang, Y. Xu, Y. Xiao, T. Li, Review of soft linear actuator and the design of a dielectric elastomer linear actuator, Acta Mech. Solida Sin. 32 (5) (2019) 566–579.

[23] J. Wang, A. Chortos, Control strategies for soft robot systems, Adv. Intell. Syst. 4 (5) (2022) 2100165.

[24] G.-Y. Gu, J. Zhu, L.-M. Zhu, X. Zhu, A survey on dielectric elastomer actuators for soft robots, Bioinspiration Biomim. 12 (1) (2017) 011003.

[25] O. Yeoh, On the Ogden strain-energy function, Rubber Chem. Technol. 70 (2) (1997) 175–182.

[26] G. Marckmann, E. Verron, Comparison of hyperelastic models for rubber-like materials, Rubber Chem. Technol. 79 (5) (2006) 835–858.

[27] K. Shimizu, T. Nagai, J. Shintake, Dielectric elastomer fiber actuators with aqueous electrode, Polymers 13 (24) (2021) 4310.

[28] S. Rosset, O.A. Araromi, J. Shintake, H.R. Shea, Model and design of dielectric elastomer minimum energy structures, Smart Mater. Struct. 23 (8) (2014) 085021.

[29] J. Zou, G. Gu, Dynamic modeling of dielectric elastomer actuators with a minimum energy structure, Smart Mater. Struct. 28 (8) (2019) 085039.

[30] P. Huang, W. Ye, Y. Wang, Dynamic modeling of dielectric elastomer actuator with conical shape, Plos One 15 (8) (2020) e0235229.

[31] Y. Zhao, G. Meng, W. Zhang, Characterization and modeling of viscoelastic hysteresis in a dielectric elastomer actuator, Smart Mater. Struct. 29 (5) (2020) 055019.

[32] F. Branz, A. Francesconi, Modelling and control of double-cone dielectric elastomer actuator, Smart Mater. Struct. 25 (9) (2016) 095040.

[33] M.G. Atia, A. Mohammad, A. Gameros, D. Axinte, I. Wright, Reconfigurable soft robots by building blocks, Adv. Sci. (2022) 2203217.

[34] M.S. Xavier, A.J. Fleming, Y.K. Yong, Finite element modeling of soft fluidic actuators: Overview and recent developments, Adv. Intell. Syst. 3 (2) (2021) 2000187.

[35] M. Russo, S.M.H. Sadati, X. Dong, A. Mohammad, I.D. Walker, C. Bergeles, K. Xu, D.A. Axinte, Continuum robots: An overview, Adv. Intell. Syst. 5 (5) (2023) 2200367.

[36] A. Alin, Minitab, Wiley Interdiscip. Rev. Comput. Stat. 2 (6) (2010) 723–727.

[37] K. Guo, Y. Zhang, J. Sun, Towards stable milling: Principle and application of active contact robotic milling, Int. J. Mach. Tools Manuf. 182 (2022) 103952.

[38] D. Wang, D. Tan, L. Liu, Particle swarm optimization algorithm: an overview, Soft Comput. 22 (2) (2018) 387–408.

[39] M.G. Atia, H. El-Hussieny, O. Salah, A supervisory-based collaborative Obstacle-Guided Path Refinement algorithm for path planning in wide terrains, IEEE Access 8 (2020) 214672–214684.

[40] M. Dehghani, S.A.A. Moosavian, Modeling and control of a planar continuum robot, in: 2011 IEEE/ASME International Conference on Advanced Intelligent Mechatronics (AIM), IEEE, 2011, pp. 966–971.

Mohamed G.B. Atia received his B.Sc. degree in mechatronics engineering from Assiut University, Egypt in 2016, and the Ph.D. form the Department of Mechanical, Materials and Manufacturing Engineering, University of Nottingham, UK in 2023.

He is currently a Research Fellow with the Department of Mechanical, Materials and Manufacturing Engineering, University of Nottingham, UK. His research interests include soft robotics, mechatronics, path planning, and exoskeletons.

Abdelkhalick Mohammad received the B.Sc. degree in mechatronics engineering from Assiut University, Assiut, Egypt, in 2006, and the M.Eng. and Ph.D. degrees from Toyohashi University of Technology, Toyohashi, Japan, in 2010 and 2013, respectively, both in robotics and mechatronics.

He is currently an Associate Professor of mechatronics with the Department of Mechanical, Materials and Manufacturing Engineering, University of Nottingham, UK. His research interests include mechatronics system design, robotics, machine tool control, and control theory.

Andres Gameros received the M.Sc. degree in Manufacturing Engineering from Monterrey Tech in collaboration with Technical University of Denmark, in 2012, and the Ph.D. degrees from Monterrey Tech, in collaboration with the University of Nottingham, in 2015.

He has been working as a Research Associate for five years, then an Assistant Professor in Intelligent Tooling and Specialist Machines with the Department of Mechanical, Materials and Manufacturing Engineering, University of Nottingham, UK for two years till Jan. 2023. He is currently working as a research & technology project engineer in Rolls-Royce plc. His research interests include fixture design, metrology, precision engineering, and uncertainty analysis.

Dragos Axinte received the M.Eng. degree in manufacturing engineering in 1988, and the Ph.D. degree in manufacturing engineering from University of Galati, Galati, Romania, in 1996.

After graduating, he was with the R&D in industry for ten years and then moved to academia to lead research in the field of machining, process monitoring and design of innovative tooling/robotics for in-situ repair especially related to on-wing repair of aeroengines. He is currently a Professor of manufacturing engineering with the Faculty of Engineering, University of Nottingham, Nottingham, UK. Since 2009, he has been the Director of Rolls-Royce University Technology Centre in manufacturing and on-wing technology, Nottingham, UK.

Prof. Axinte is a Fellow of the International Academy of Production Engineering (FCIRP). He is also the Editor-in-Chief of the *International Journal of Machine Tools and Manufacture*.

Iain Wright received his Mechanical Engineering degree from the University of Derby, UK, in 2000. He is currently the Manufacturing Senior Specialist for Automation & Robotics in Rolls-Royce plc. He is a Chartered Engineer and Fellow of the Institution of Manufacturing Engineers, and his research interests are mechatronics, automation and robotics.